Text S14. Evidence against electrostatic repulsion in phosphoryl transfer transition states

Because of the extreme resilience of phosphate esters to hydrolysis, early on it was proposed that electrostatic repulsion between the incoming nucleophile and the phosphate ester in the transition state hinders the reaction [33,34]. However, two subsequent studies bear directly on this question and provide evidence that electrostatic repulsion from formal charge on the incoming nucleophile does not significantly hinder phosphoryl transfer. The reactivity of both neutral and negatively charged oxygen nucleophiles with negatively charged phosphorylated 4-methyl pyridine fall on the same correlation line versus nucleophile pK_a [35-37], providing evidence against significant electrostatic repulsion in the transition state for the oxyanion reactions. In addition, increasing the ionic strength had only a 5-fold differential effect on the reaction rates of an oxyanion nucleophile versus a neutral nucleophile [36], providing no indication of strong electrostatic repulsion in the transition state.

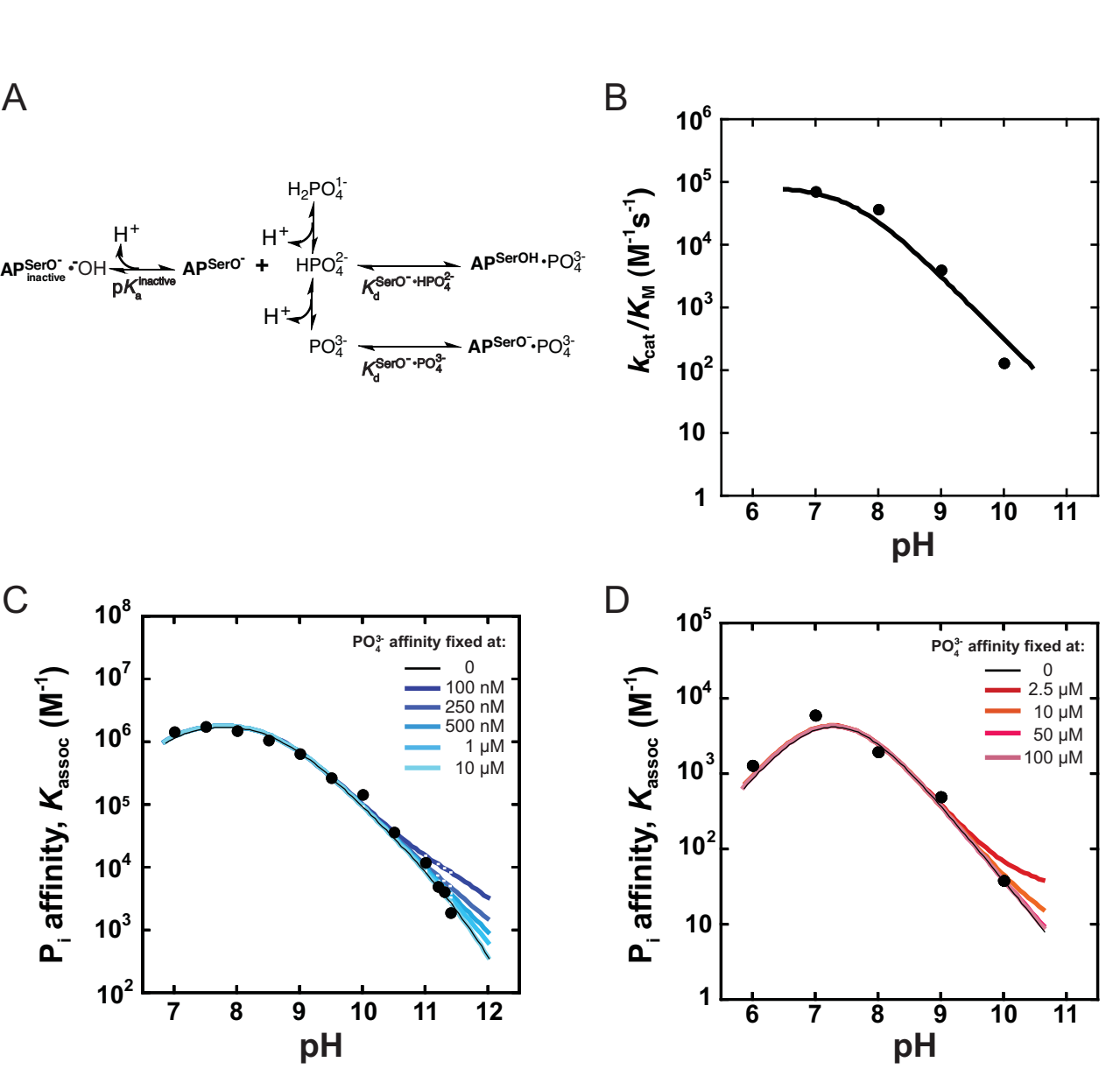
A
B
C
D
pH
pH
pH
pH
affinity fixed at:
affinity fixed at:
0
100 nM
250 nM
500 nM
1 µM
10 µM
0
2.5 µM
10 µM
50 µM
100 µM

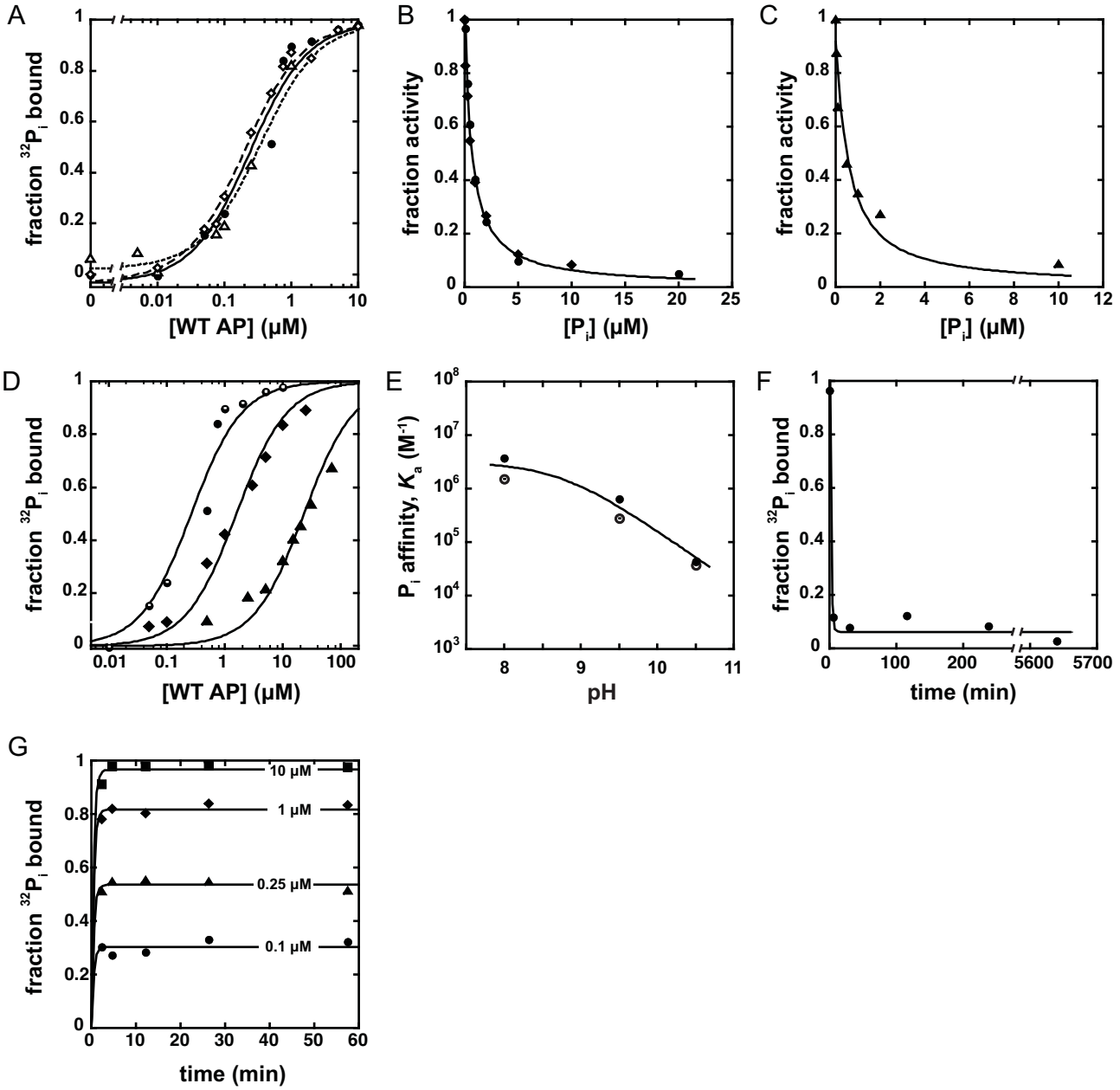
A
fraction $^{32}P_i$ bound
[WT AP] (μM)
B
fraction activity
$[P_i]$ (μM)
C
fraction activity
$[P_i]$ (μM)
D
fraction $^{32}P_i$ bound
[WT AP] (μM)
E
P_i affinity, K_a (M^{-1})
pH
F
fraction $^{32}P_i$ bound
time (min)
G
fraction $^{32}P_i$ bound
10 μM
1 μM
0.25 μM
0.1 μM
time (min)

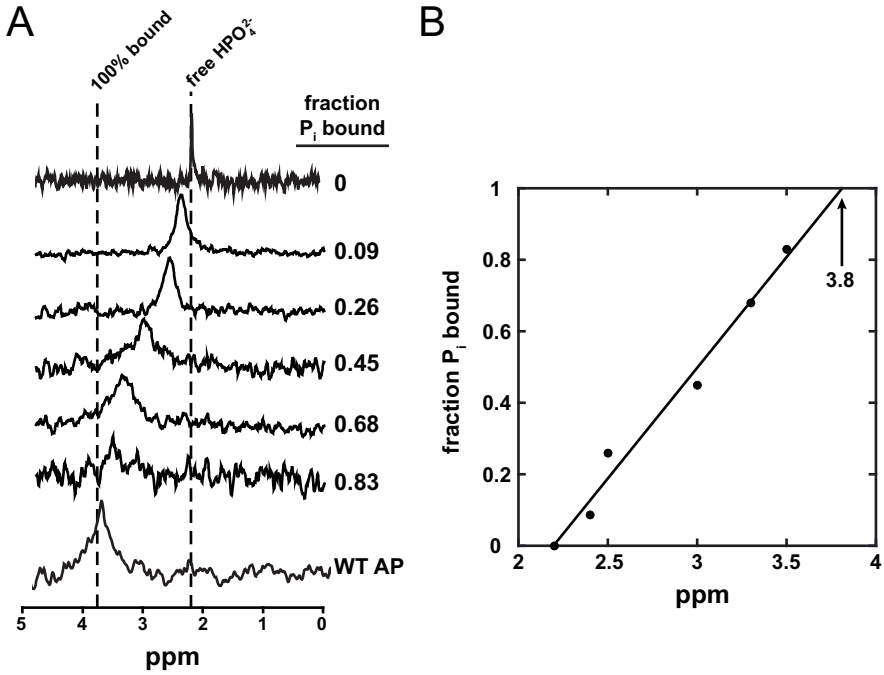
A
100% bound
free HPO_4^{2-}
fraction P_i bound
0
0.09
0.26
0.45
0.68
0.83
WT AP
5
4
3
2
1
0
ppm
B
fraction P_i bound
1
0.8
0.6
0.4
0.2
0
2
2.5
3
3.5
4
3.8
ppm

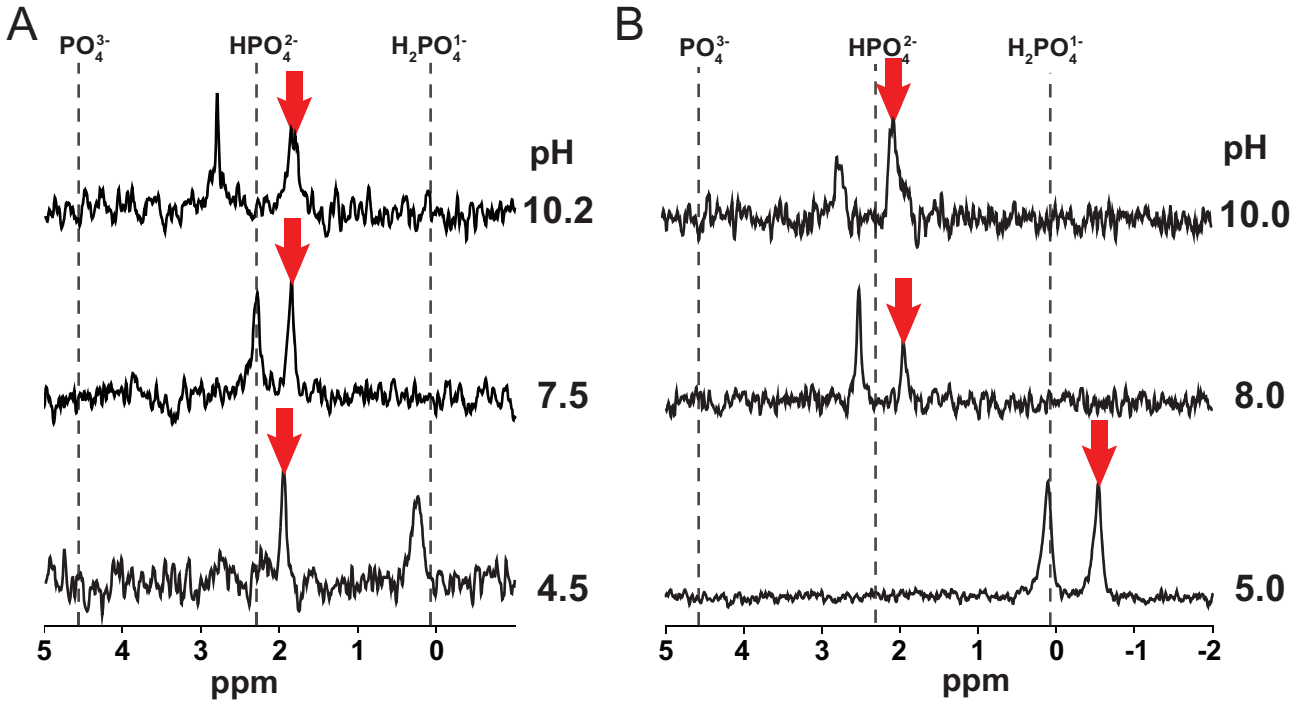
A
PO_4^{3-}
HPO_4^{2-}
$H_2PO_4^{1-}$
pH
10.2
7.5
4.5
5
4
3
2
1
0
ppm
B
PO_4^{3-}
HPO_4^{2-}
$H_2PO_4^{1-}$
pH
10.0
8.0
5.0
5
4
3
2
1
0
-1
-2
ppm

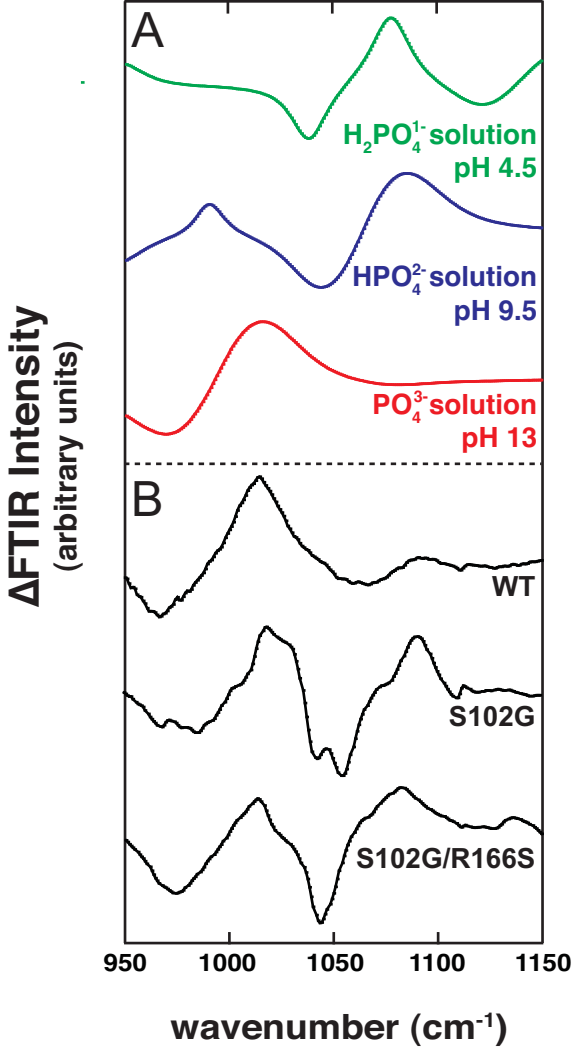
A
$H_2PO_4^{1-}$ solution
pH 4.5
HPO_4^{2-} solution
pH 9.5
PO_4^{3-} solution
pH 13
B
WT
S102G
S102G/R166S
950
1000
1050
1100
1150
wavenumber (cm^{-1})
ΔFTIR Intensity
(arbitrary units)

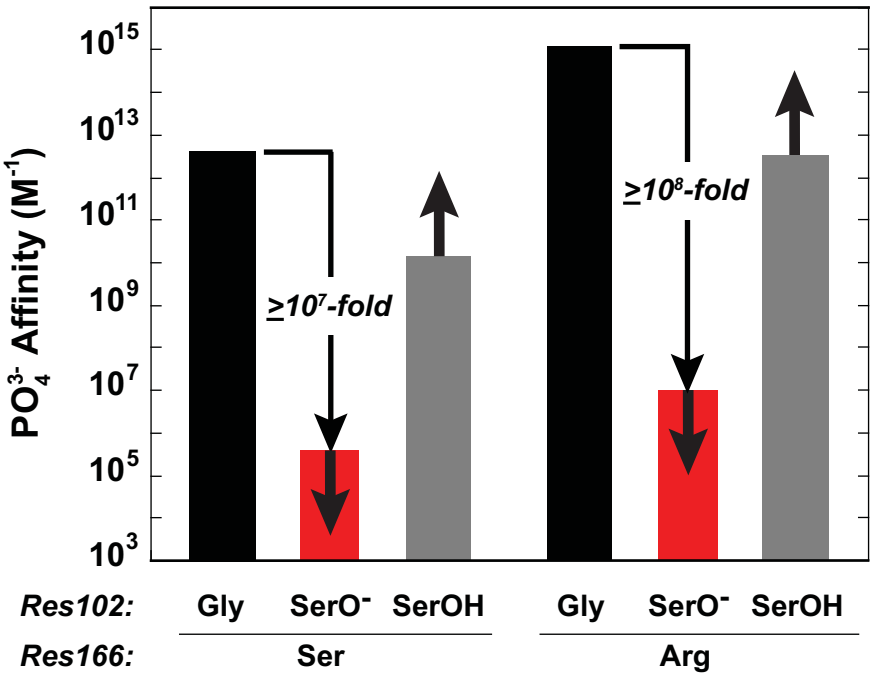
PO_4^{3-} Affinity (M^{-1})
10^{15}
10^{13}
10^{11}
10^{9}
10^{7}
10^{5}
10^{3}
≥10^{7}-fold
≥10^{8}-fold
Res102:
Gly
SerO⁻
SerOH
Gly
SerO⁻
SerOH
Res166:
Ser
Arg

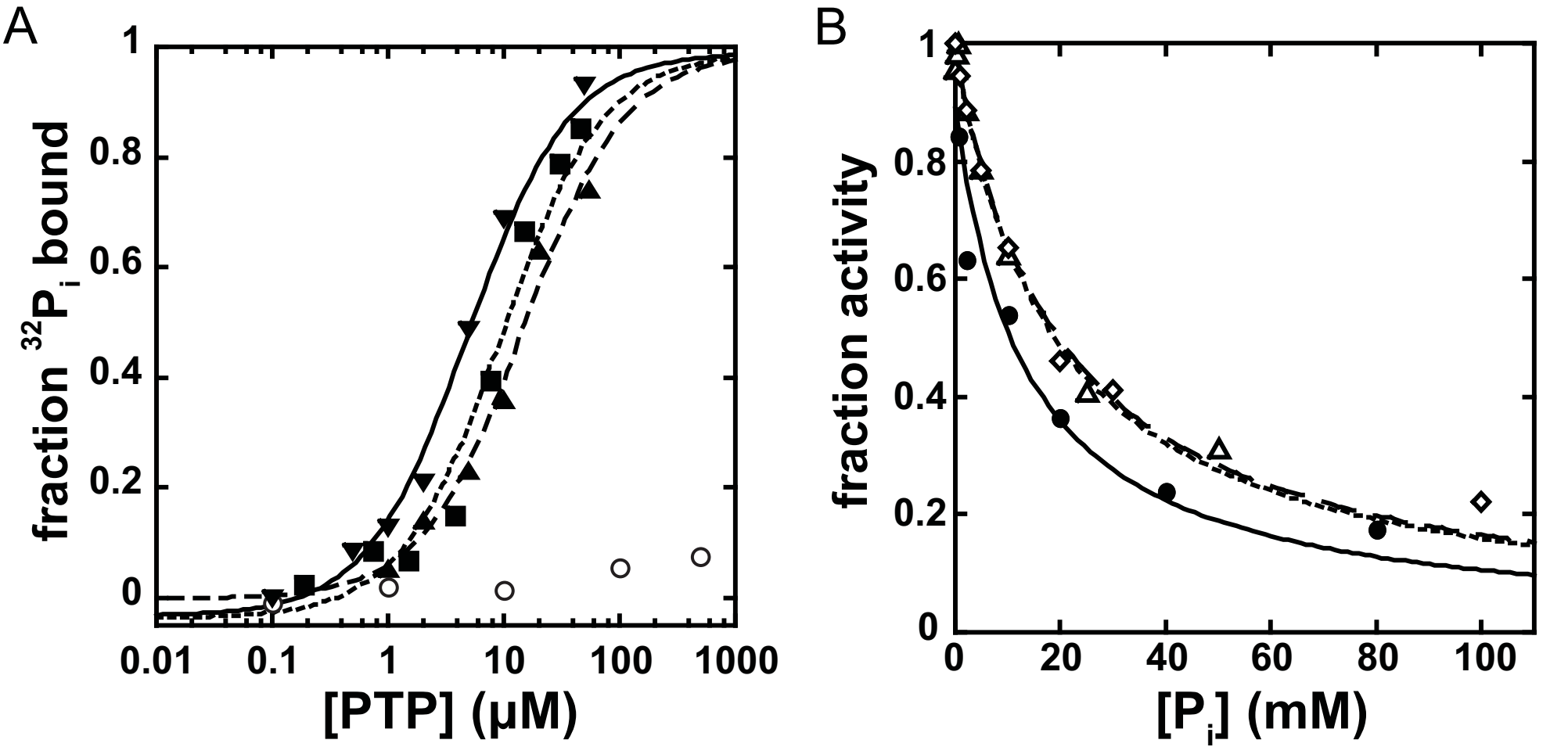
A
fraction $^{32}P_i$ bound
1
0.8
0.6
0.4
0.2
0
0.01
0.1
1
10
100
1000
[PTP] (μM)
B
fraction activity
1
0.8
0.6
0.4
0.2
0
0
20
40
60
80
100
[P_i] (mM)

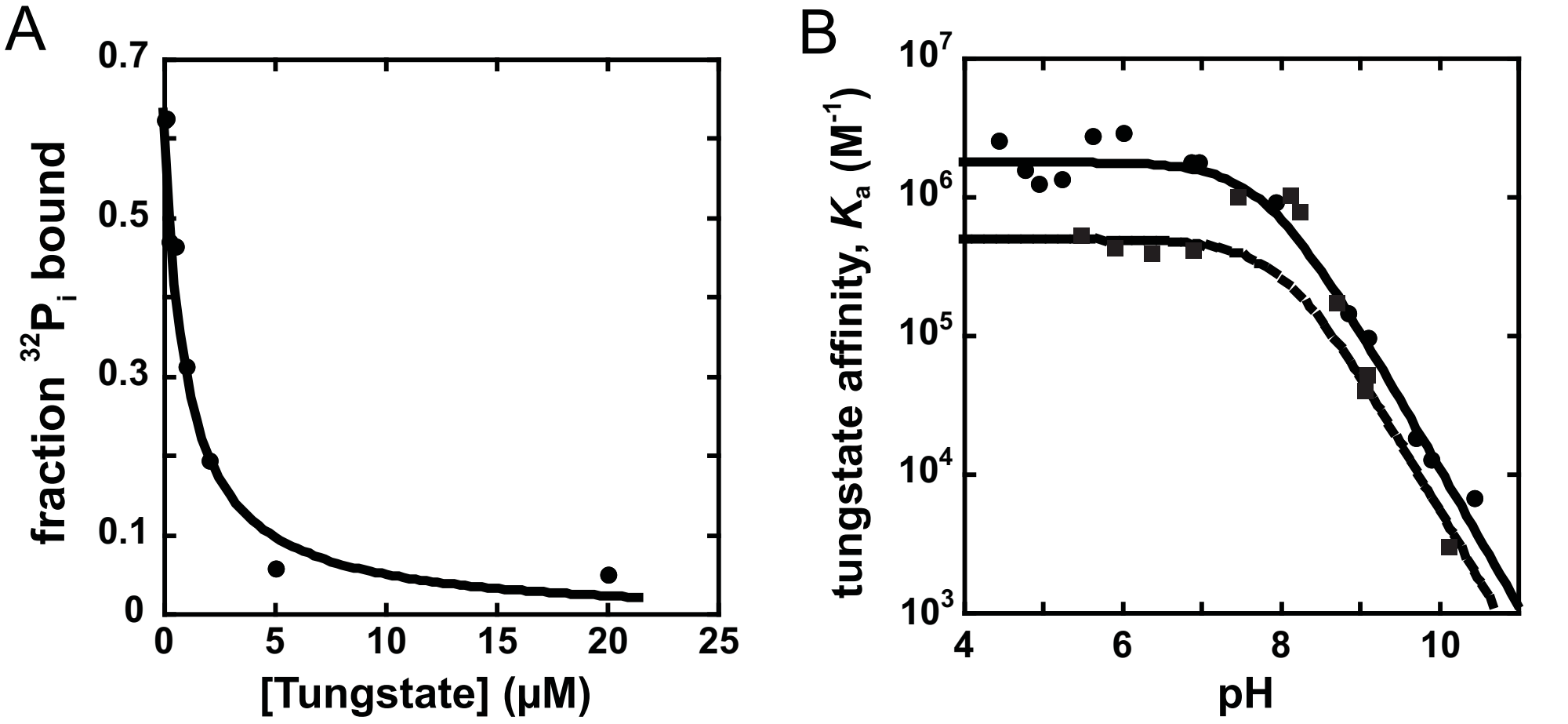
A
0.7
0.5
0.3
0.1
0
fraction $^{32}P_i$ bound
0
5
10
15
20
25
[Tungstate] (μM)
B
10^7
10^6
10^5
10^4
10^3
tungstate affinity, K_a (M^{-1})
4
6
8
10
pH

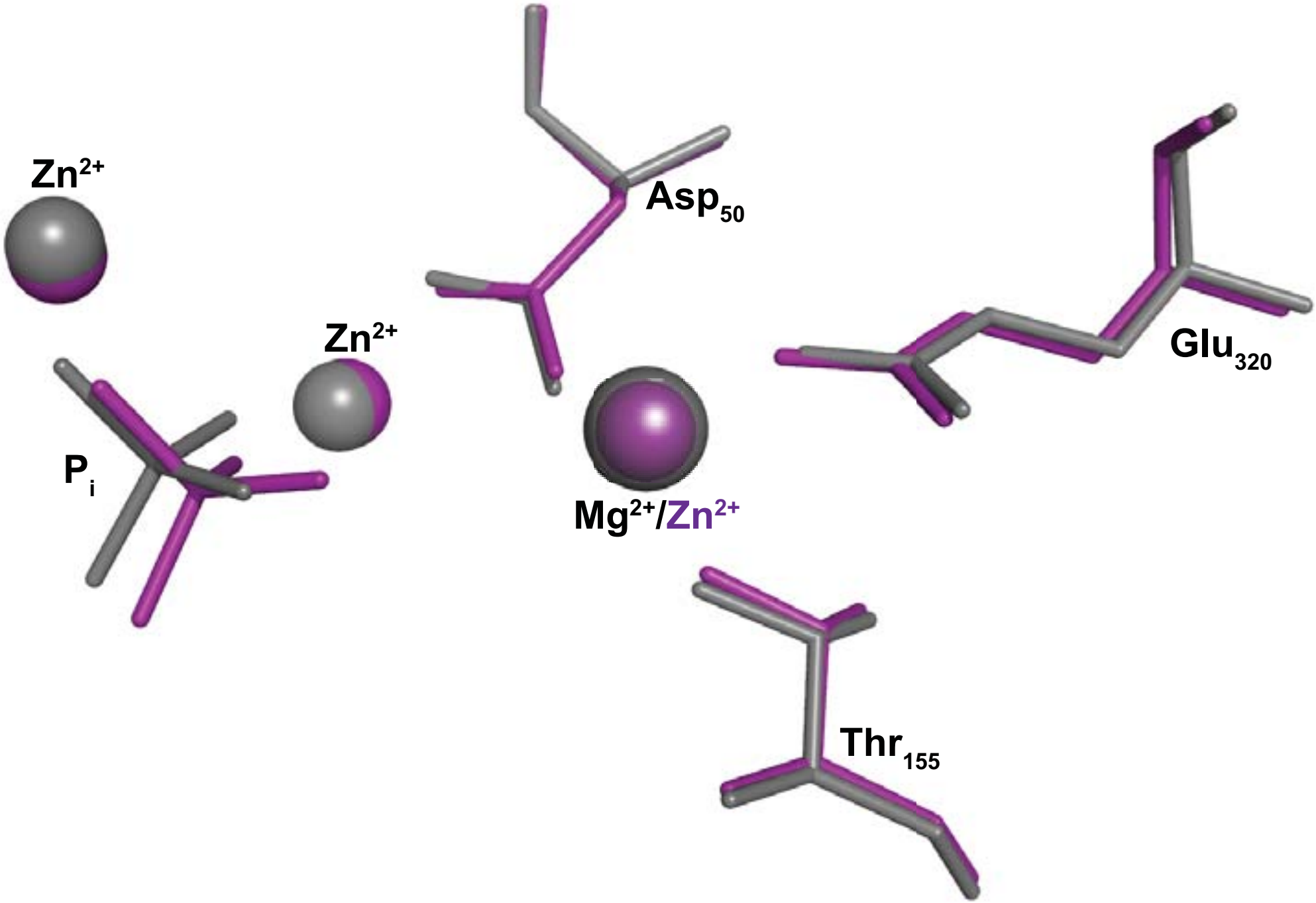
Zn^{2+}
Zn^{2+}
P_i
Asp_{50}
Mg^{2+}/Zn^{2+}
Glu_{320}
Thr_{155}

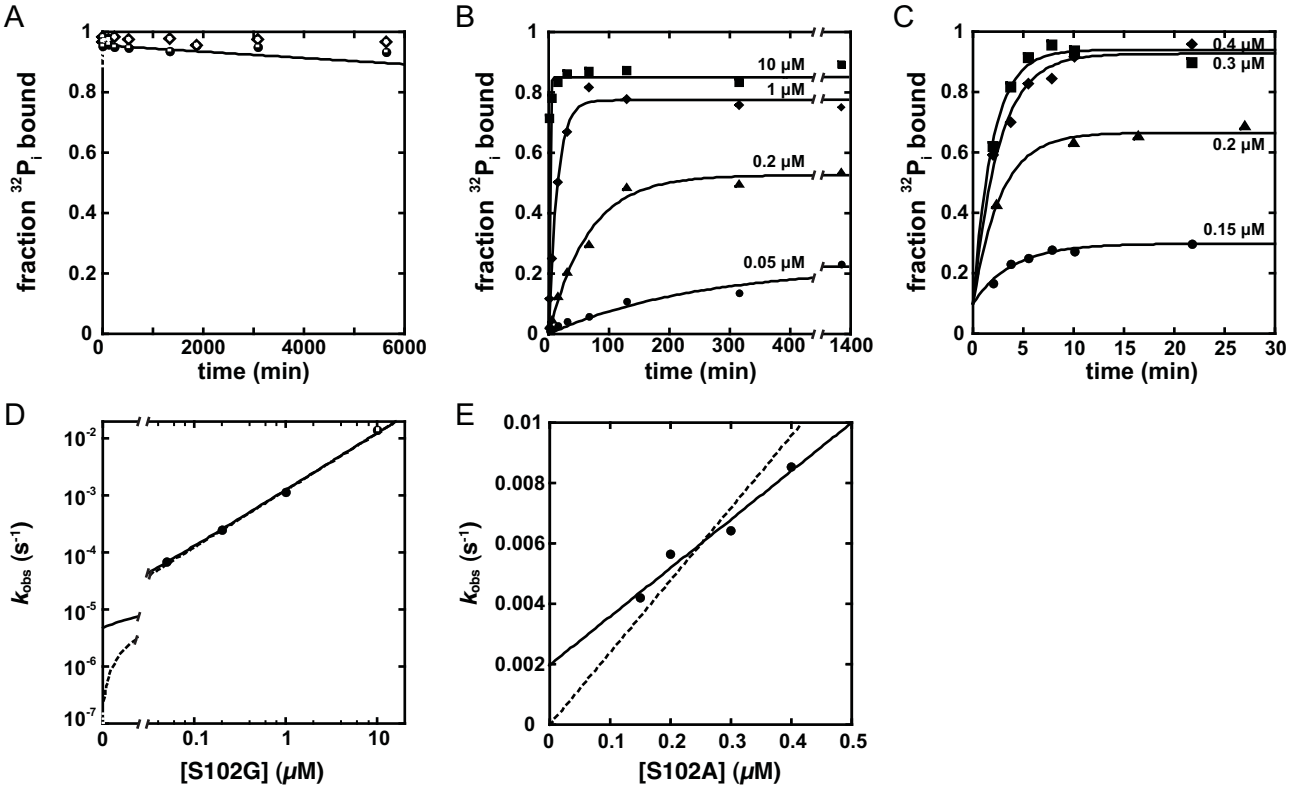
A
fraction $^{32}P_i$ bound
time (min)
B
10 μM
1 μM
0.2 μM
0.05 μM
C
0.4 μM
0.3 μM
0.2 μM
0.15 μM
D
k_{obs} (s^{-1})
[S102G] (μM)
E
k_{obs} (s^{-1})
[S102A] (μM)

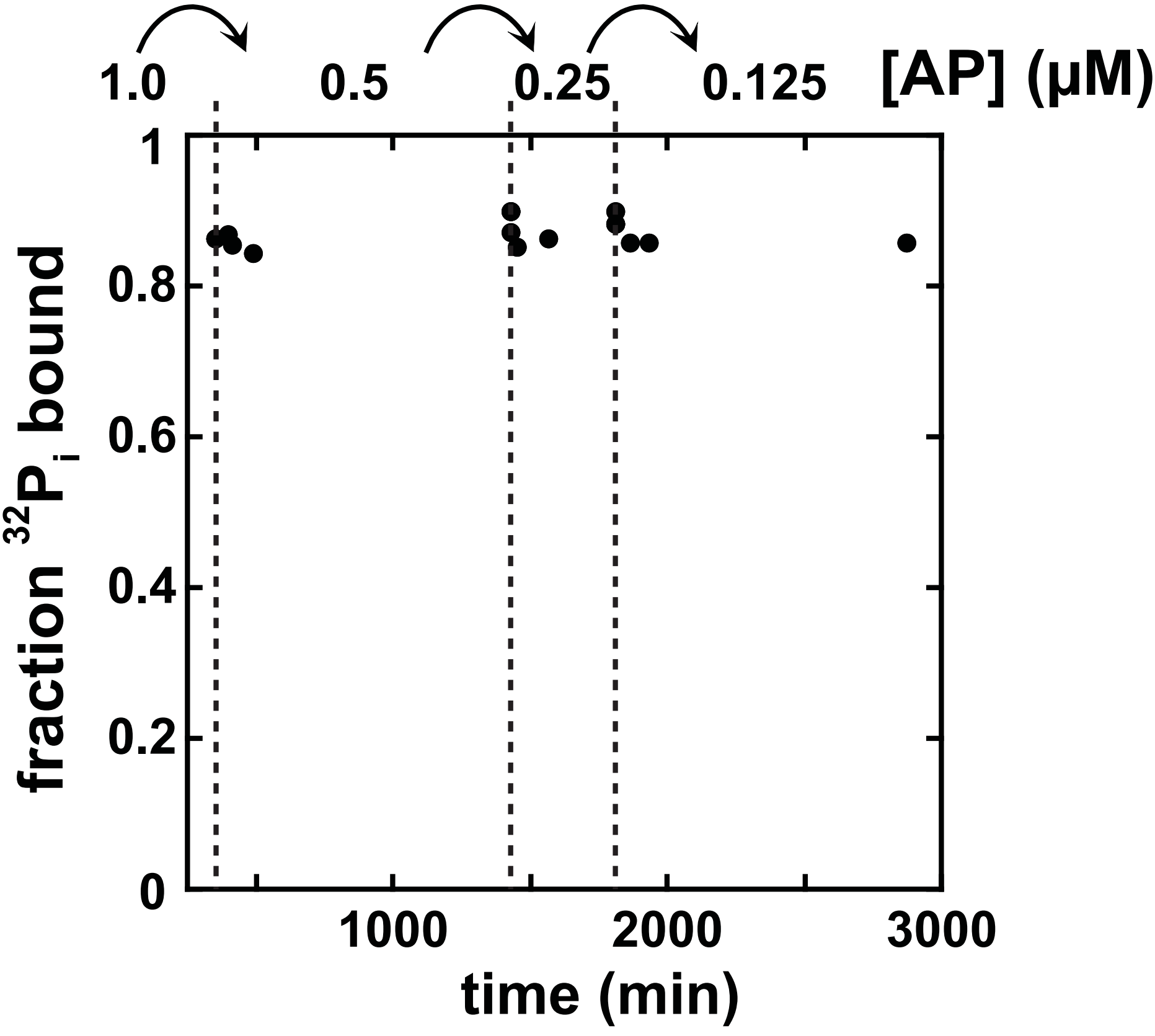
1.0
0.5
0.25
0.125
[AP] (μM)
1
0.8
0.6
0.4
0.2
0
fraction $^{32}P_i$ bound
1000
2000
3000
time (min)

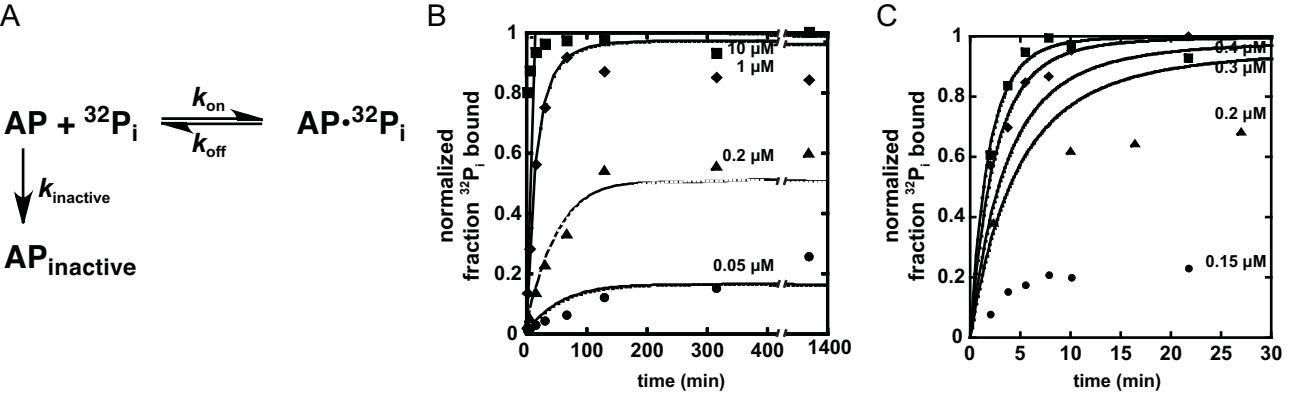
A
AP + 32Pi
kon
koff
AP•32Pi
kinactive
APinactive
B
normalized fraction 32Pi bound
time (min)
10 µM
1 µM
0.2 µM
0.05 µM
C
normalized fraction 32Pi bound
time (min)
0.4 µM
0.3 µM
0.2 µM
0.15 µM

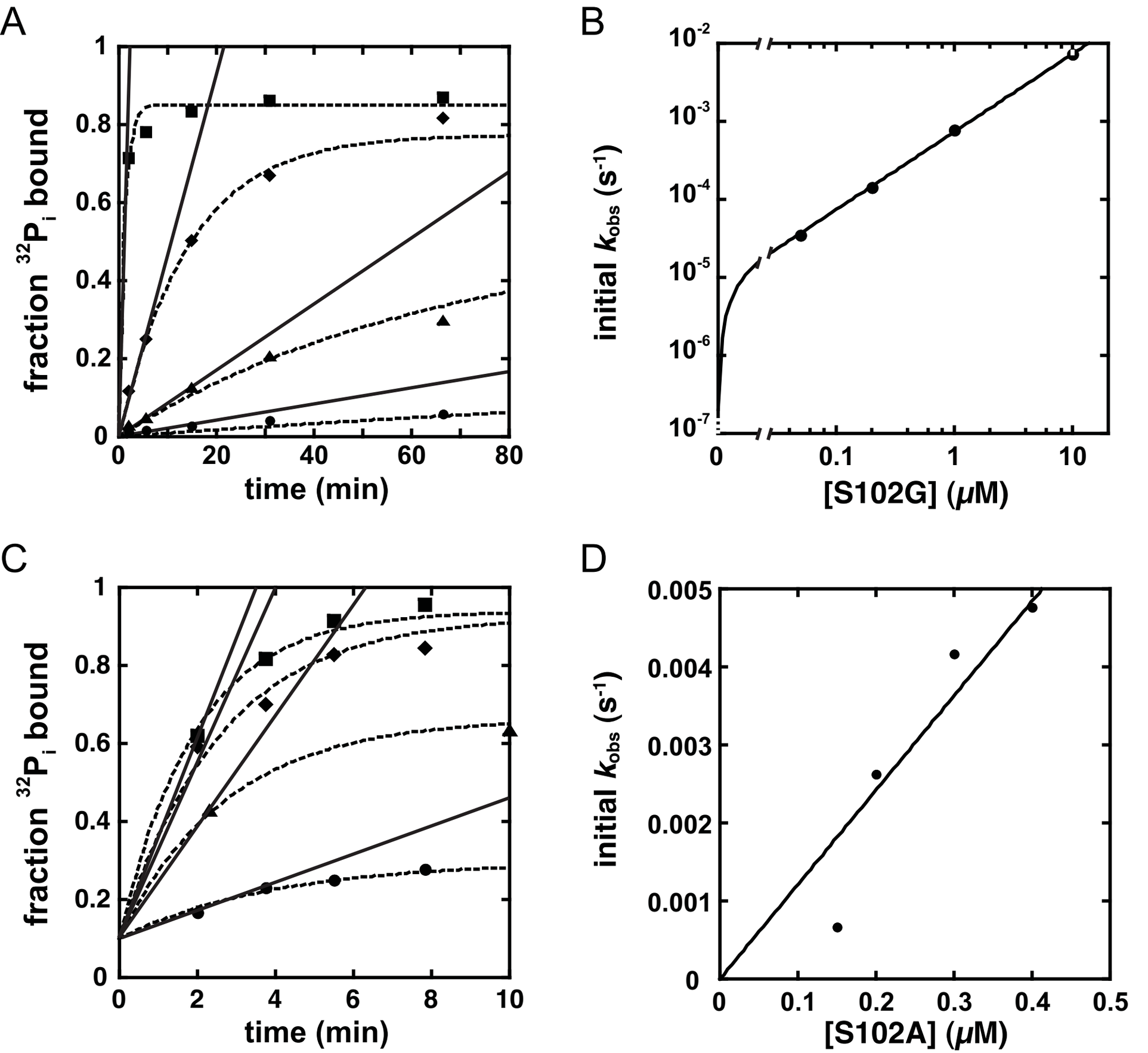
A
fraction $^{32}P_i$ bound
time (min)
B
initial k_{obs} (s^{-1})
[S102G] (μM)
C
fraction $^{32}P_i$ bound
time (min)
D
initial k_{obs} (s^{-1})
[S102A] (μM)

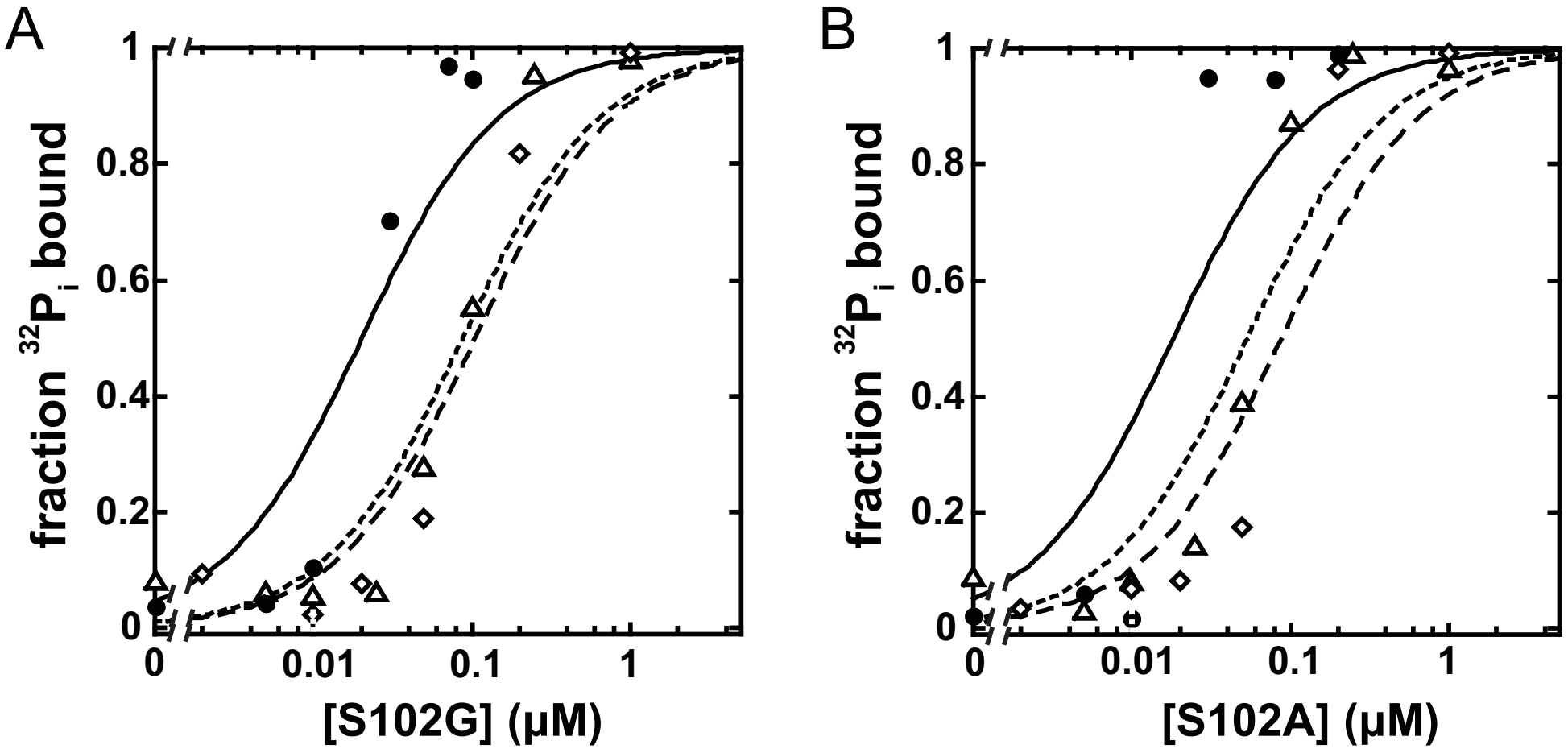
A
B
fraction $^{32}P_i$ bound
1
0.8
0.6
0.4
0.2
0
0
0.01
0.1
1
[S102G] (μM)
[S102A] (μM)

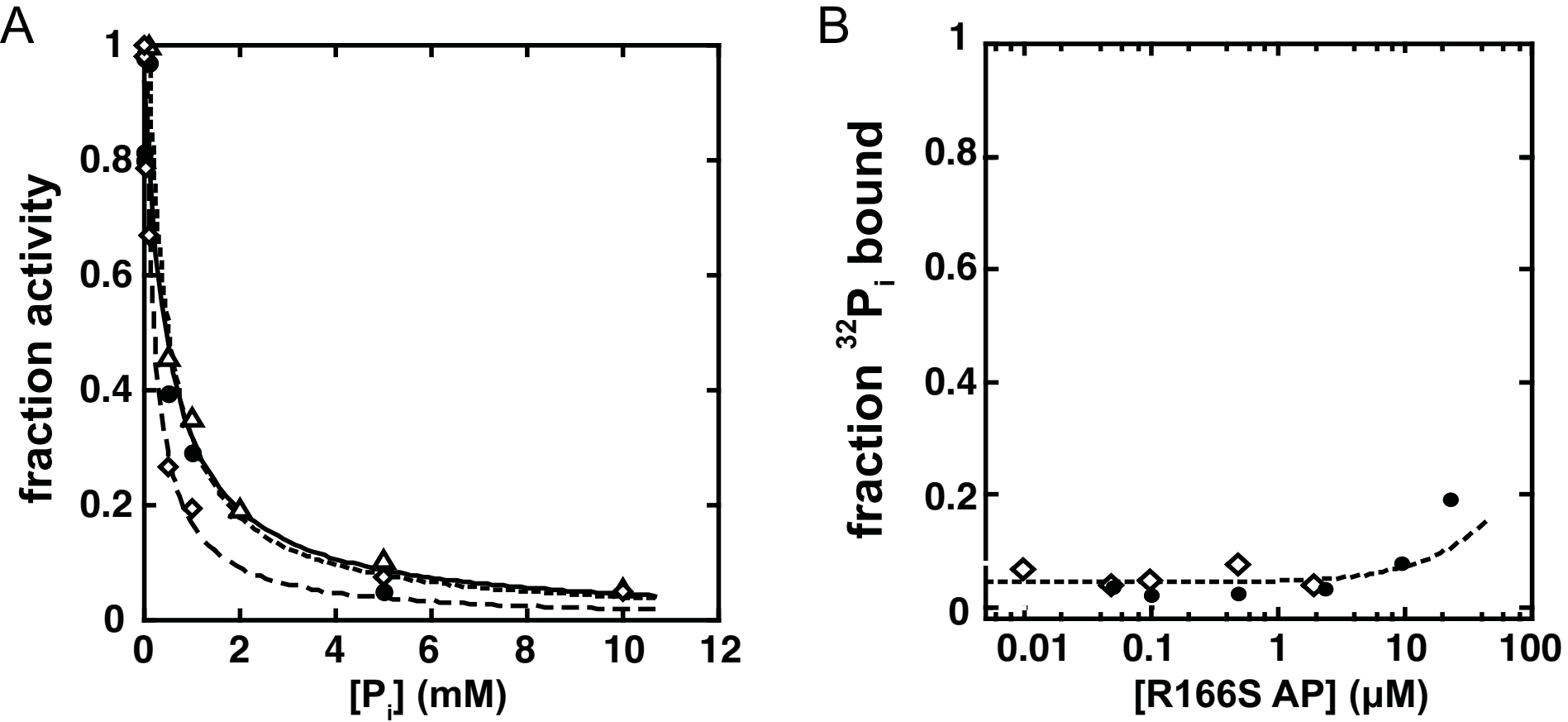
A
fraction activity
1
0.8
0.6
0.4
0.2
0
0
2
4
6
8
10
12
[P$_i$] (mM)
B
fraction $^{32}P_i$ bound
1
0.8
0.6
0.4
0.2
0
0.01
0.1
1
10
100
[R166S AP] (μM)

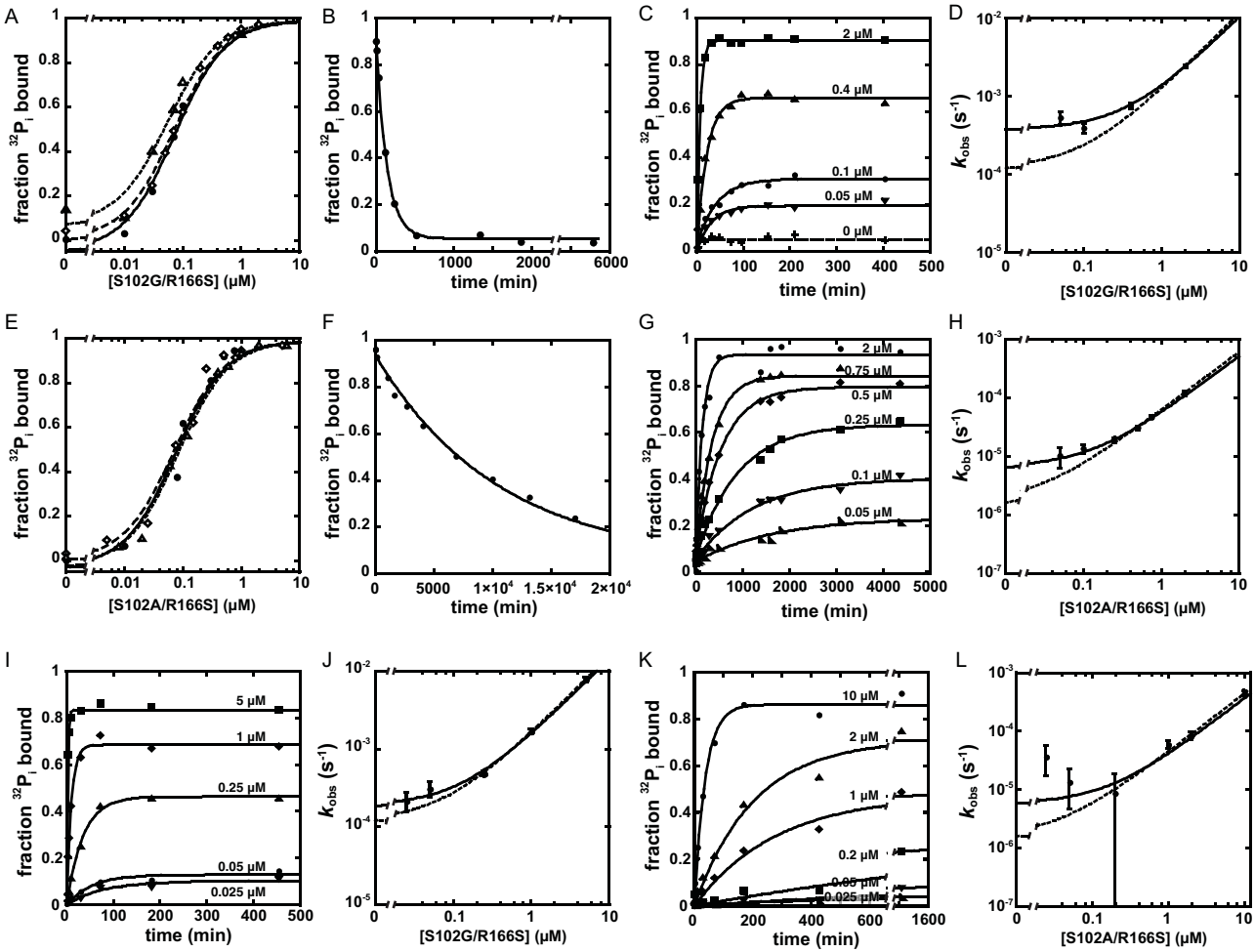
A
B
C
D
E
F
G
H
I
J
K
L
fraction $^{32}P_i$ bound
k_{obs} (s^{-1})
[S102G/R166S] (μM)
[S102A/R166S] (μM)
time (min)
2 μM
0.4 μM
0.1 μM
0.05 μM
0 μM
0.75 μM
0.5 μM
0.25 μM
5 μM
1 μM
0.025 μM
10 μM
0.2 μM

Table S1. Summary of P_i binding kinetics for WT, S102G, S102A, R166S, S102G/R166S, and S102A/R166S AP

AP	k_{on}[(a)] ($M^{-1}s^{-1}$)	k_{off}^{chase}[(b)] (s^{-1})	k_{off}^{chase}/k_{on} (nM)	K_d^{obs}[(c)] (nM)	K_{rel}^{obs}[(d)]
WT	-	≥0.1	-	260 (±74)	(1)
S102G	~1000	$\leq 2\times10^{-7}$	≤0.2	-	≥1000
S102A	$\sim 1\times10^{4}$	$\leq 2\times10^{-7}$	≤0.02	-	$\geq 1\times10^{4}$
R166S	-	-	-	$(3.6 \pm 1.6)\times10^{5}$	(1)
S102G/R166S	1190 (±120)	$(1.2 \pm 0.05)\times10^{-4}$	103 (±15)	66 (±8)	5500
S102A/R166S	51 (±4)	$(1.6 \pm 0.06)\times10^{-6}$	32 (±4)	77 (±6)	4700

[a] k_{on} for S102G and S102A AP is the estimated association rate constant from a fit analysis of the $^{32}P_i$ uptake assay results described in Text S2. k_{on} for S102G/R166S and S102A/R166S AP is from the fit of the k_{obs} values from the uptake assay versus the [AP] shown in Figure S8D and H. [b] k_{off}^{chase} is the dissociation rate constant measured by the $^{32}P_i$ chase assay (Figure S1F; Figure S2A; Figure S8B and F). [c] K_d^{obs} is the dissociation constant for P_i binding at pH 8.0 measured from the fraction $^{32}P_i$ bound after an incubation time sufficient to reach equilibrium (Figure S1A for WT AP; Figure S8A for S102G/R166S; Figure S8D for S102A/R166S AP), except for the value reported for R166S AP, which is from kinetic inhibition assays (Figure S7A). [d] The K_{rel}^{obs} value is calculated by dividing the dissociation constant for AP with Ser102 intact by the dissociation constant (K_d^{obs}) for the Ser102 mutants in either the context of WT or R166S AP; larger values represent stronger binding of the Ser102 mutant relative to proteins with Ser102 intact.

Table S2. Crystallographic data and model statistics

	S102G/R166S AP
Data collection	
Beamline	SSRL 11-1
Wavelength (Å)	0.9795
Space group	$P6_322$
Unit cell dimensions (Å)	
a	160.935
b	160.935
c	139.549
Resolution range (Å)	50-2.8
Effective resolution (Å) (I / σ=2)	50-2.9
No. of total reflections	4,616,524
No. of unique reflections	26,488
Completeness (highest-resolution shell)	99.2 (98.5)
Redundancy (highest-resolution shell)	20.4 (19.4)
I / σ (highest-resolution shell)	7.3 (1.5)
R_{merge} (%)[a]	33.7
Refinement statistics	
R-factor (R_{free}) (%)[b]	23.2 (29.6)
No. of protein atoms	6546
No. of solvent atoms	0
No. of ligand atoms	16
Average *B*-factor	21.5
RMSD bond lengths (Å)	0.013
RMSD bond angles (°)	2.6

[a] $R_{merge} = \sum |I_{obs} - I_{ave}| / \sum I_{obs}$

[b] *R*-factor = $\sum ||F_o| - |F_c|| / \sum |F_o|$ See the work of Brunger for a description of R_{free}; ref. [25]

Table S3. ^{31}P NMR chemical shift summary of free P_i and P_i bound to WT, R166S, S102G, and S102G/R166S AP

Protein-Bound P_i AP Species	**pH**	**^{31}P NMR chemical shift (ppm)**
WT	5.0-9.0	3.7
R166S	7.5	3.8
S102G	4.5-10.2	1.94
S102G/R166S	>8.0	1.94
S102G/R166S	<5.0	-0.74
Free P_i Species[(a)]		
$H_2PO_4^{1-}$	4.0	0.05
HPO_4^{2-}	7.5	2.19
PO_4^{3-}	13.0	4.64

[a] Chemical shifts reported for unbound P_i species were measured here under conditions identical to those used for protein-containing samples and referenced to a 1% phosphoric acid standard. These shifts are within error of those reported previously [28]. At intermediate pH values the observed chemical shift represents a weighted average of the ionic forms present.

Text S1. Observed activity of Ser102 mutants likely arises from WT AP contamination

AP mutants with the Ser102 nucleophile removed have been reported to retain a low level of phosphate monoester hydrolysis activity [1,2]. However, our results provide strong evidence that this activity arises from contaminants in the mutant preparations.

The reported activity of the Ser102 mutant preparations from different laboratories vary by 40-fold under similar conditions. Values for k_{cat}/K_M for the hydrolysis of *p*-nitrophenyl phosphate (*p*NPP) by S102A AP of 30 $M^{-1}s^{-1}$ [1], 1.3×10^3 $M^{-1}s^{-1}$ [2], and 10-1000 $M^{-1}s^{-1}$ from preparations in our lab have been observed. Observation of these kinetic parameters would require WT AP to be present at only 0.01-0.0001% [$(k_{cat}/K_M)^{WT\ AP} \sim 1\times10^7$ $M^{-1}s^{-1}$; e.g., [3-6]]. The prior studies of S102A AP gave inhibition constants for P_i that were similar to the inhibition constant obtained for WT AP in these studies (K_i = 15 and 30 μM in [1] measured for WT and S102A AP, respectively; K_i = 5.6 ± 0.7 μM and 7.9 ± 0.3 μM in [2] measured for WT and S102A AP, respectively), as would be expected if a small fraction of WT AP were responsible for the observed activity. These reported K_i values are greater than the actual dissociation constant for P_i binding to WT AP likely because the *p*NPP substrate was present at concentrations greater than its K_M and because inhibiting concentrations of P_i would have been generated in the course of the reaction (see ref. [6]).

The results of our current study provide additional, strong evidence that the Ser102 mutant enzymes are not responsible for the observed activity. Our P_i binding results indicate that the Ser102 mutants would be strongly inhibited even with sub-micromolar levels of P_i (K_i values at pH 8 range from ≤0.02 – 80 nM for the Ser102 mutants used herein; see Table 1 and Table S1). For example, the amount of P_i giving half-inhibition in the prior studies (~10 μM) would give a least 10^5-fold inhibition ($K_i \leq 0.02$ nM with S102A AP; Table S1), not the 2-fold inhibition that

was observed. Further, spectroscopic activity assays of phosphate monoesters [6] require substrate concentrations that would produce highly inhibitory concentrations of P_i and thus result in minimal turnover and strong curvature if the activity arose from the mutant AP; e.g., full turnover of 200 nM of *p*NPP, resulting in the production of 200 nM P_i, gives a change of only 0.003 AU (ε_{400}^{max}=16,652 $M^{-1}cm^{-1}$ for *p*-nitrophenolate at pH 8.0), which is near or below typical spectrophotometer noise levels. Thus, even if the mutant APs have some residual activity, negligible product accumulation would be observed from their activity, and thus, the reported and observed activities must arise from contaminating activities.

Text S10. Comparison of AP•P_i affinities with AP Ser102 protonated, deprotonated, or mutated to Gly

Most simply, it was expected that the PO_4^{3-} affinities of AP with Ser102 removed by mutation or with Ser102 neutralized by protonatation would be approximately equal because both result in the removal of the proposed destabilizing anion and electrostatic repulsion. The PO_4^{3-} affinity of AP with protonated Ser102 was computed using a thermodynamic cycle (Figure 5A) involving the observed P_i affinity at pH 8.0, the HPO_4^{2-} pK_a, and the upper limit of the Ser102 pK_a. Because the Ser102 pK_a is an upper limit (≤5.5; [6]), the PO_4^{3-} dissociation constant values calculated using the thermodynamic cycle are upper limits, with $K_d^{SerOH•PO_4^{3-}}$ of ≤69 pM and ≤290 fM for R166S and WT AP, respectively (Table 2 and Figure S13; grey bars). Assuming the simplest model, that the Ser102 pK_a is 5.5, gives affinities in the same range as those for the S102G mutants (Figure S13; cf. black and grey bars) but the PO_4^{3-} affinity of AP with Ser102 protonated is somewhat lower (~10^2-fold) than the PO_4^{3-} affinity of AP with Ser102 mutated. The structural comparisons of WT and variant APs in Figure 3 show that Ser102, which is likely protonated in these structures, displaces P_i when Arg166 is not present to buttress P_i in the preferred WT binding mode. This observation suggests that protonated Ser102 may retain some fractional destabilization effect on P_i binding. Alternatively, if the Ser102 pK_a is actually lower, ~3.5 instead of 5.5, then the calculated PO_4^{3-} affinity of AP with Ser102 protonated would be the same as the PO_4^{3-} affinity of AP with Ser102 mutated.

Text S11. Previous estimation for the destabilization from Ser102 on the binding of a dianionic phosphate

A previous estimate of the dianionic substrate destabilization from Ser102 was obtained by first comparing the dissociation constants for PO_4^{3-} binding to WT AP with Ser102 deprotonated (see Figure S9C; $K_d^{SerO^-\bullet PO_4^{3-}} \geq 100$ nM) and to WT AP with Ser102 neutralized by protonation (see Figure 5; $K_d^{SerOH\bullet PO_4^{3-}} \leq 290$ fM) yielding a destabilization of $\geq 3.4\times10^5$-fold, which corresponds to a free energy difference of ≥7.5 kcal/mol [$\Delta\Delta G = RT\ln(K_d^{SerO^-\bullet PO_4^{3-}} / K_d^{SerOH\bullet PO_4^{3-}})$] [7]. To estimate the destabilization from Ser102 on dianion binding it was assumed that the destabilization from Ser102 on PO_4^{3-} trianion binding scaled with the charge difference between a trianion and a dianion, such that the dianion destabilization was calculated to be two-thirds of the trianion destabilization in energetic terms [≥5 kcal/mol = (-2/-3)×(≥7.5 kcal/mol)]; this value would correspond to a binding destabilization for a dianion of $\geq 4.8\times10^3$-fold. This value assumed that the destabilization from Ser102 scales log-linearly with the charge of the P_i ligand, but this relationship need not hold. Nevertheless, the current work shows that the Ser102 destablization of trianion binding is $\geq 10^8$-fold and that the destabilization of dianion binding is $\geq 10^3$-fold, similar to the prior estimate. In energetic terms, trianion binding is destabilized by ≥10.9 kcal/mol [$= RT\ln(\geq 10^8)$] and dianion binding is destabilized by ≥4.1 kcal/mol [$= RT\ln(\geq 10^3)$]. Because these values are both limits we cannot determine the difference in the Ser102 destabilization for dianion versus trianion binding.

Text S12. Estimation of the contribution of Arg166 to binding of P_i dianion

The dissociation constant for HPO_4^{2-} binding the S102G AP mutant with Arg166 present is very likely lower than the dissociation constant determined for HPO_4^{2-} binding the S102G/R166S AP mutant ($K_d^{Gly \bullet HPO_4^{2-}}$ = 90 nM; Table 2) due to favorable contacts between the nonbridging oxygen atoms of HPO_4^{2-} and Arg166. However, the very strong binding of PO_4^{3-} by S102G AP with K_d ~ 1 fM masked our ability to measure HPO_4^{2-} binding. We conservatively estimate that Arg166 contributes an additional ~10-fold to the binding of HPO_4^{2-} based on 1) its previously measured contribution to stabilization of the dianionic phosphoserine intermediate (E-P species) of 90-fold [8] and 2) structural evidence showing Arg166 in position to hydrogen bond with the oxygen atoms of bound HPO_4^{2-} [29,30]. In the simplest scenario, we expect HPO_4^{2-} to bind in the presumed substrate binding orientation with a proton in place of the leaving group monoester portion of the substrate, as illustrated in Figure 7. In this orientation, Arg166 can make hydrogen bonds to both nonbridging oxygen atoms of the bound dianion that are deprotonated. However, the HPO_4^{2-} proton could occupy one of the phosphate oxygen atoms that is expected to hydrogen bond to Arg166. In this scenario we still expect Arg166 to contribute to binding because functional studies show that Arg166 contributes ~40-fold to the catalysis of methyl-*p*NPP hydrolysis in which the methyl group is attached to one of the phosphate oxygen atoms that would ordinarily contact Arg166 [9]. This result suggests that Arg166 can make a significant binding contribution of at least 10-fold even if the bound ligand disrupts one of the hydrogen bonds from Arg166.

Text S13. Comparison of HPO_4^{2-} and PO_4^{3-} binding by S102G AP

The binding results and analysis in the main text provide estimates for the strong binding of both HPO_4^{2-} and PO_4^{3-} by S102G/R166S and S102G AP but with much stronger binding of PO_4^{3-}. We have measured this differential affinity for S102G/R166S as 4.3×10^5-fold (Table 2; $K_d^{Gly\bullet PO_4^{3-}} / K_d^{Gly\bullet HPO_4^{2-}}$ for S102G/R166S AP), and a somewhat larger differential affinity of $\sim10^7$-fold is expected with Arg166 present in the S102G AP mutant (Table 2; $K_d^{Gly\bullet PO_4^{3-}} / K_d^{Gly\bullet HPO_4^{2-}}$ for S102G AP). Presumably, PO_4^{3-} binds more strongly than HPO_4^{2-} because each of the three anionic oxygen atoms of PO_4^{3-} has more charge to interact with the positively charged AP active site residues (-0.75 vs. -0.67 formal charge per oxygen for PO_4^{3-} and HPO_4^{2-}, respectively). In addition, the fourth oxygen atom of HPO_4^{2-} is protonated, has no formal charge, and likely makes weaker electrostatic interactions relative to the analogous oxygen atom of PO_4^{3-}, although it is not known which oxygen atom of the dianion is protonated. The large binding affinity preference of AP for the more negatively charged PO_4^{3-} shown here is consistent with previous work with AP that showed a very steep increase in catalytic activity for substrates with increasing negative charge [31].

Text S2. Tests of the new equilibrium-binding assay with WT AP

The affinity of ground state ligands for AP is typically determined by measuring inhibition of catalytic activity (with *p*NPP, or sometimes *p*-nitrophenyl sulfate, *p*NPS) under conditions in which the observed K_i equals the K_d for ligand binding (e.g., [6-9]). To obtain accurate measurements of P_i binding, the overall turnover of the substrate, which results in the generation of P_i, should be less than the K_i value of P_i. When more P_i is generated during the course of the reaction, the enzyme is subject to additional product inhibition and the observed inhibited activity is a complex combination of the amount of P_i added and the amount generated during the assay. For WT AP, the *p*NPP substrate concentration used during inhibition measurements (~0.5 μM) is kept near, but below the observed K_i for P_i binding (0.5-1 μM) at pH 8.0, thereby avoiding substantial product inhibition even when the reaction is allowed to go to completion while enabling a change in absorbance that can be accurately followed (full turnover of 0.5 μM of substrate results in a 0.008 AU change; ε_{400}^{max} =16,652 $M^{-1}cm^{-1}$ for *p*-nitrophenolate at pH 8.0).

The observed binding of P_i to the Ser102 AP mutants at pH 8.0 is much stronger than to WT AP. Consequently, to accurately measure the P_i affinity of these mutants, much less substrate would need to be used. Unfortunately, as noted above, the limits of detecting product require substrate concentrations of at least 0.2-0.5 μM. As shown herein, the inhibition constant for P_i at pH 8.0 is ≤0.2 nM for the S102G and S102A AP mutants and ~75 nM for the S102G/R166S and S102A/R166S AP mutants, preventing measurement via inhibition of activity. As also noted above (Text S1), there is no evidence of any measurable activity from the Ser102 mutants of AP and the activity that is observed likely arises from trace WT AP contamination.

To measure P_i binding to the Ser102 mutants a new equilibrium-binding assay was developed. The details of this assay are described in the Methods section of the main text. Briefly, the assay entails incubating various concentrations of AP with trace $^{32}P_i$. The bound and unbound populations of AP are then separated using a centrifugal filter, and the fraction $^{32}P_i$ bound is measured using scintillation counting of the filtrate and the retentate.

To test the validity of this assay, several controls were carried out. First, the fraction of $^{32}P_i$ bound to WT AP was plotted as a function of the WT AP concentration and the data fit to a simple binding isotherm. Figure S1A shows three replicate binding assays. The dissociation constant obtained was ~2-fold lower than that from previous measurements using inhibition of activity, agreement that is reasonable given the errors in these assays and the difficulty of obtaining accurate measurements in the kinetic assay due to the low substrate concentrations needed (K_d = 0.26 ± 0.074 μM from the new equilibrium-binding assay, Figure S1A; K_d = 0.61 ± 0.1 μM from kinetic inhibition assays of *p*NPP and *p*NPS, Figure S1B and C).

To further test the new equilibrium-binding assay, the P_i affinity of WT AP was measured at higher pH. The binding of P_i by WT AP was previously shown to be pH-dependent [6,7] (see also Figure S9C): as the pH is raised from ~8, the observed P_i affinity decreases log linearly with a slope of -1. The results using the new assay for P_i binding to WT AP at pH 8.0, 9.5, and 10.5 are shown in Figure S1D, and the K_d values are plotted in Figure S1E along with the previously determined values measured by kinetic inhibition [7]. The results agree well, demonstrating that the new assay is capable of measuring the AP•P_i affinities as weak as ~10 μM.

As an additional test of the new equilibrium-binding assay, the kinetics of P_i release and uptake were measured using this assay. To measure P_i release, $^{32}P_i$ was first incubated with a

concentration of WT AP high enough to achieve near-complete $^{32}P_i$ binding. After this incubation, an excess of unlabeled P_i (≥2 mM) was added and the fraction $^{32}P_i$ bound was assessed at different times after this unlabeled P_i chase. As shown in Figure S1F, all of the $^{32}P_i$ was released before the first time point after the addition of unlabeled P_i, giving a lower limit of the release rate constant, k_{off}, of ≥0.01 s^{-1}, consistent with an estimate of $k_{off} \sim 10$ s^{-1} from previous studies [10-12]. Analogous results were obtained for the kinetics of $^{32}P_i$ uptake (Figure S1G), which is also expected to be fast relative to the time resolution of the assay. (The observed uptake for a reversible binding process is the sum of $k_{on}[AP] + k_{off}$ [13]: for 0.1 μM AP, $k_{obs} = (0.1\ \mu M)k_{on} + 10\ s^{-1}$ and the expected k_{on} value is $\sim 1\times10^7\ M^{-1}s^{-1}$ [5,6,14]. Thus, the expected k_{obs} at this protein concentration is 11 s^{-1} –a value that is faster than the time resolution of the assay used here and consistent with the limit of $k_{obs} \geq 0.03\ s^{-1}$ established by the data in Figure S1G.)

Further controls of the assay with Ser102 mutant versions of APs and with R166S AP described below provide additional evidence that the results of the assay accurately reflect P_i binding.

Text S3. Equilibrium-binding assay results with S102G and S102A AP

The equilibrium-binding assay was used to obtain limits for the P_i binding affinity of the AP Ser102 mutants S102G and S102A. We first sought to determine the timescale needed to achieve equilibrium binding. The observed rate constant for binding equilibration equals k_{on}[AP] + k_{off} [13] so we sought to determine k_{off}. After incubation of the mutant proteins at a concentration shown to result in nearly 100% $^{32}P_i$ bound, a chase assay was conducted by adding excess unlabeled P_i, such that any $^{32}P_i$ that dissociates would be replaced by unlabeled P_i. No significant dissociation of $^{32}P_i$ from S102G or S102A AP was observed even after approximately 100 hours (Figure S2A). This result is in contrast to the rapid dissociation observed for WT AP (Figure S1F). These results suggest that the dissociation of P_i from S102G or S102A AP (k_{off}) is slower than 2×10^{-7} s^{-1}.

We next measured the uptake kinetics of $^{32}P_i$ by these AP mutants. P_i-free S102G or S102A AP (0.05-10 μM of S102G AP; 0.15-0.4 μM of S102A AP) was combined with ~200 pM $^{32}P_i$ and the fraction $^{32}P_i$ bound was measured over time. The observed increases in fraction $^{32}P_i$ bound at various protein concentrations were fit to yield k_{obs} values and the endpoint fraction $^{32}P_i$ bound at each protein concentration (Figure S2B and C for S102G and S102A AP, respectively). Given the extremely slow dissociation of $^{32}P_i$ indicated by the chase assays described above, it was expected that for each protein concentration used in these uptake assays, the endpoint fraction $^{32}P_i$ bound would plateau at the maximum fraction bound as long as the rate constant for binding, k_{on}, were greater than ~4 $M^{-1}s^{-1}$ [e.g., if $k_{off}^{chase} \leq 2\times10^{-7}$ s^{-1} and $k_{on} \geq 4$ $M^{-1}s^{-1}$ then the dissociation constant ($K_d = k_{off}/k_{on}$) would be ≤0.05 μM]. Fits to the observed uptake rate constant, k_{obs}, versus the [AP] have slopes that give apparent k_{on} values, with values of 1300 and 1.6×10^4 $M^{-1}s^{-1}$ for S102G and S102A AP, respectively (Figure S2D and E). However, even

though these values are greater than 4 $M^{-1}s^{-1}$, the endpoint amounts of bound $^{32}P_i$ plateau well below the maximum achievable fraction $^{32}P_i$ bound.

To investigate this limited uptake of P_i, 1 μM of S102G AP that had completed $^{32}P_i$ uptake at 0.85 fraction $^{32}P_i$ bound was diluted several times to reach a final S102G AP concentration of 0.125 μM. This concentration in the uptake assay (Figure S2B) resulted in less than half of the $^{32}P_i$ bound, but the results from the chase assay predict that reducing the S102G AP concentration by dilution would not significantly decrease the fraction $^{32}P_i$ bound because, once bound, $^{32}P_i$ does not dissociate over this timeframe (Figure S2A). Re-equilibration to lower fraction $^{32}P_i$ bound did not occur upon dilution (Figure S3), consistent with the expectations based on the chase assay and suggesting a complexity associated with uptake.

A general model to account for the unexpectedly low fraction $^{32}P_i$ binding during the uptake assay is that the amount of free protein capable of binding $^{32}P_i$ decreases over the assay time, due to denaturing events, as depicted by the model in Figure S4A. We carried out simulations and nonlinear regression fitting using the KinTek Explorer simulation program [15,16], allowing both a reversible $^{32}P_i$ binding equilibrium and an irreversible loss of free, bindable protein according to the scheme of Figure S4A. The k_{off} value was fixed as the limiting value from the chase assay. A global fit of this model to the uptake data for all of the S102G AP concentrations (Figure S4B) indicates that a model with irreversible inactivation of free AP but not AP•P_i can account for the reduced P_i binding at the lower protein concentrations. Values of ~1000 $M^{-1}s^{-1}$ and ~3×10^{-4} s^{-1} for k_{on} and $k_{inactive}$ for S102G AP are obtained. The k_{on} value was used in combination with the limit for k_{off}^{chase} from the chase assay of ≤2×10^{-7} s^{-1} to provide a limit for the dissociation constant for P_i binding ($K_d = k_{off}^{chase}/k_{on}$) of ≤0.2 nM (as reported in Table S1 and

Table 1 in the main text). This affinity is ≳1000-fold higher than the WT AP affinity with Ser102 intact (K_{rel}^{obs}; Table 1 and Table S1).

The model of Figure S4A did not yield a good fit to the uptake data for the S102A AP mutant (Figure S4C), particularly at the lower concentrations of S102A AP, presumably due to a less predictable loss of activity. We therefore used the initial uptake data points for S102G and S102A to estimate the k_{on} value before the potential protein inactivation process would significantly contribute to the observed uptake. As shown in Figure S5, the initial rates of $^{32}P_i$ uptake were estimated by fitting the initial data points at each protein concentration to a line. These initial uptake rate constants were plotted versus the concentration of protein to yield second-order rate constants reflecting the initial uptake. For S102G this was ~700 $M^{-1}s^{-1}$ (Figure S5B), in reasonable agreement with the association rate constant estimated from the global fit of the model in Figure S4A (~1000 $M^{-1}s^{-1}$). The initial uptake value estimated for S102A was ~1×10^4 $M^{-1}s^{-1}$ (Figure S5D), suggesting that k_{on} for this process is ~10-fold faster compared to that for S102G AP. Using this value for k_{on} in combination with the limit for k_{off}^{chase}, yields a crude estimated limit for the K_d of P_i binding by S102A AP of ≲0.02 nM (Table 1 and Table S1).

Replicate binding assays for S102G and S102A AP showed unexpected high variability in the fraction $^{32}P_i$ bound at the endpoint (Figure S6), whereas the other AP variants with weaker binding and faster equilibration gave highly reproducible results (e.g. Figure S1A for WT AP; Figure S8A for S102G/R166S AP; and Figure S8E for S102A/R166S AP) and the kinetics of P_i uptake and dissociation for S102G/R166S and S102A/R166S AP agree well with equilibrium-binding measurements (see below and Table S1). The complications for S102G and S102A AP presumably result from an inactivation process that is not fully reproducible. The lack of P_i dissociation observed with S102G and S102A AP indicates very strong binding and we turned to

S102G/R166S and S102A/R166S AP for quantitative analysis, as the behavior of these mutants was reproducible and self-consistent.

Text S4. Equilibrium binding of P_i to R166S, S102G/R166S, and S102A/R166S AP

We determined the P_i binding affinity of the R166S, S102G/R166S, and S102A/R166S AP variants. Previous measurements of the R166S AP mutant P_i affinity by kinetic inhibition gave K_i values of 400-500 μM at pH 8.0 [8,17], and we obtained a value of K_d = 360 μM using this kinetic assay (Figure S7A), in reasonable agreement with the prior measurements. Attempts at measuring the R166S AP affinity by the equilibrium-binding method developed here resulted in a significant decrease in flow rate during filtration with concentrations of R166S AP above 25 μM, suggesting that the filter membrane may become partially blocked with protein. As expected for this mutant, no significant binding was observed over the lower R166S AP concentrations that were accessible in this assay, and the slightly higher than expected binding at 25 μM may have arisen from nonspecific effects related to the above-noted protein blockage (Figure 7B).

We were able to use the equilibrium-binding assay to measure the P_i affinities of S102G/R166S and S102A/R166S AP, and this assay was required given the absence of detectable activity of these mutants (Text S1). The fraction $^{32}P_i$ bound to each mutant after incubation times in which the fraction $^{32}P_i$ no longer changed was plotted against the concentration of protein to generate binding curves with dissociation constants for P_i binding of 66 and 77 nM for S102G/R166S and S102A/R166S AP, respectively at pH 8.0 (Figure S8A and E; Table 1; Table S1). Repeat measurements showed very good reproducibility (Figure S8A and E), in contrast to the high variability observed with S102G and S102A AP (Figure S6).

As an additional control, measurement of the kinetics of P_i binding gave a calculated dissociation constant ($K_d = k_{off}/k_{on}$) that was similar to the dissociation constant measured with the equilibrium-binding assay. The dissociation rate constant for each mutant was measured using the chase assay described above (Figure S8B and F). Fits to the observed decrease in the fraction

$^{32}P_i$ bound (see Methods) yielded k_{off}^{chase} values of 1.2×10^{-4} and 1.6×10^{-6} s^{-1} for S102G/R166S and S102A/R166S AP, respectively. The time-dependent uptake of $^{32}P_i$ was also measured for these mutants. Fits to the uptake yielded k_{obs} values and the maximal fraction of $^{32}P_i$ bound (Figure S8C and G). The uptake data fit well to a two-state binding model in which $k_{obs} = k_{on}[AP] + k_{off}$ ($AP+{}^{32}P_i \rightleftharpoons AP\bullet{}^{32}P_i$), (Figure S8D and H), yielding k_{on} of 1400 and 36 $M^{-1}s^{-1}$ for S102G/R166S and S102A/R166S AP, respectively. The y-intercept of these fits, which in principle reflect the dissociation rate constant (k_{off}), has a high uncertainty because small changes in the fit slope result in relatively large changes to the y-intercept value. Despite the fit error, the y-intercept values from the uptake assay were in reasonable agreement (within 2-4 fold for S102G/R166S and S102A/R166S AP, respectively) with the k_{off} values measured more accurately with the chase assay above.

Dissociation constants calculated from the kinetic rate constants and from the fraction $^{32}P_i$ bound at endpoints were within 2-fold of one another (Table S1), consistent with simple two-state binding such that K_d equals k_{off}/k_{on}.

The k_{on}^{uptake} values are several orders of magnitude below the expected value for a diffusion-limited process (10^7-10^8 $M^{-1}s^{-1}$; k_{on} for WT AP is ~1×10^7 [8,10]), as also suggested by the limited data for S102G and S102A AP above. Slow binding to some proteins has been attributed to slow dissociation of water (or ions) from the binding site [18-24], and the high density of positively charged residues, enhanced by removal of the Ser102 anion, may result in a site that is particularly recalcitrant to exchange of solvent out of the active site.

Text S5. Interplay between Ser102 and Arg166 revealed by structural comparison

When Ser102 and Arg166 are both present (WT AP), P_i is positioned in a binding mode akin to that of the vanadyl transition state analog. When Arg166 is mutated to serine (R166S AP), the bound P_i is rotated and the phosphorus center is translated 1.0 Å relative to its position in WT AP (Figure 3C) [8]. One model to account for the P_i binding mode in R166S AP is that in the absence of Arg166, Ser102 displaces P_i from the preferred binding mode. In these structures, Ser102 is likely protonated, but its presence may nevertheless have some destabilizing influence on bound P_i as suggested by the structural comparison in Figure 3C. This model accounts for the observation that removal of Ser102 from R166S AP (to give S102G/R166S AP) allows bound P_i to return to the WT position, akin to the vanadyl transition state analog position.

The above structural comparison suggests that Arg166 is needed to position P_i when Ser102 is present. As the P_i position is very similar to that of the vanadyl transition state analog (Figure 3A), this conclusion is consistent with a previous energetic analysis indicating that Arg166 plays a role in specific transition state stabilization [8]. The new observation that Arg166 is not needed to position P_i when Ser102 is absent (Figure 3D) provides structural support for a destabilizing ground state effect from the Ser102 nucleophile.

Text S6. Estimation of PO_4^{3-} affinity for AP with Ser102 deprotonated

The PO_4^{3-} affinity for deprotonated Ser102 AP can be estimated by measuring the P_i affinity across a pH range. In principle, the observed P_i binding at a given pH can reflect the binding contributions of any of the P_i species. The results presented in the main text indicate that the observed P_i affinity in the neutral pH range for R166S AP (and for WT AP as shown in Figure S9C and published previously [6,7]) reflects the formal binding of HPO_4^{2-}. The binding of free HPO_4^{2-} is presumably accompanied by a net internal proton transfer to give neutral Ser102 and bound PO_4^{3-} as shown by the equilibrium defined by $K_d^{SerO^- \bullet HPO_4^{2-}}$ in Figure S9A. As the pH approaches the pK_a of HPO_4^{2-} (11.7), the proportion of PO_4^{3-} in solution increases and the overall observed P_i affinity can start to reflect a direct binding contribution from PO_4^{3-}, if that affinity is sufficiently strong ($K_d^{SerO^- \bullet PO_4^{3-}}$ in Figure S9A); an increase in the observed P_i affinity as the pH is raised would indicate a binding contribution from PO_4^{3-}. The size of this contribution will depend on the solution pH and the PO_4^{3-} affinity relative to the HPO_4^{2-} affinity. As all of the Ser102 AP will be deprotonated at these pH values (p$K_a \leq 5.5$; [6]), PO_4^{3-} binding that increases as pH increases would be to AP with Ser102 deprotonated.

The observed pH-dependent P_i binding to AP is complicated by an inactivating pK_a (p$K_a^{inactive}$) associated with free AP. Nevertheless, this inactivating titration can be accounted for (using pH-dependent tungstate binding measurements as described in the main text) and if PO_4^{3-} makes a binding contribution at higher pH values, an upward trend is expected. To ensure that AP remains functional even at high pH values, *p*NPP hydrolysis activity throughout the pH range was measured, and as *p*NPP has no titratable protons in this pH range it was expected that a continuous log-linear decrease in activity reflecting only p$K_a^{inactive}$ would be observed. A

continuous log-linear decrease in activity was observed to pH 11.4 for WT AP [6,7] and to pH 10 for R166S AP (Figure S9B).

The P_i affinity data from pH 7.0-11.4 for WT AP and pH 6-10 for R166S AP are shown in Figure S9C and D, respectively. No upward-trend from PO_4^{3-} binding was detected. Thus, we could set a lower limit for $K_d^{SerO^- \bullet PO_4^{3-}}$. To estimate this value, Equation S3, derived from the model in Figure S9A, was used to fit the pH-dependent data with $K_d^{SerO^- \bullet HPO_4^{2-}}$ and $pK_a^{inactive}$ fixed based on the fits assuming HPO_4^{2-} binding only. The PO_4^{3-} affinity in Equation S3 was fixed at a series of decreasing $K_d^{SerO^- \bullet PO_4^{3-}}$ values (Figure S9C and D). Clear deviations from the high pH data are observed if $K_d^{SerO^- \bullet PO_4^{3-}}$ is set to values lower than 100 nM for WT AP and lower than 2.5 μM for R166S AP, so these values give conservative lower limits (i.e., $K_d^{SerO^- \bullet PO_4^{3-}} \geq 100$ nM and 2.5 μM for WT and R166S AP, respectively; Table 2).

Text S7. ^{31}P NMR of the R166S AP•P_i complex suggests bound PO_4^{3-}

Vibrational spectroscopy of P_i associated with WT AP allowed assignment of PO_4^{3-} as the bound species [7]. Analogous experiments with R166S AP were not successful because of low signal-to-noise even at high enzyme concentrations (3.3 mM). We therefore could not use vibrational spectroscopy to assign the P_i species bound to R166S AP as was done previously for WT AP [7]. We instead assigned the P_i species bound to R166S AP by comparing the ^{31}P NMR spectra of R166S and WT AP, as follows.

The ^{31}P NMR spectrum of P_i with WT AP at pH 8.0 shows a chemical shift of ~3.7 ppm (Figure S10A) (see also [11,26,27]). Based on the vibrational data noted above, this P_i species was assigned as PO_4^{3-} [7]. If PO_4^{3-} were also bound to R166S AP, a similar ^{31}P NMR chemical shift for the bound P_i would be expected in the simplest case. The chemical shift observed for P_i in the presence of R166S AP (Figure S10A) varies depending on the fraction of P_i that is bound (K_d value of 360 μM at pH 8.0; Figure S7A). The exchange of R166S AP-bound and unbound P_i is fast, estimated as ~6×10^4 s^{-1} (= $k_{exchange} = k_{on}$[R166S AP] + k_{off} = $(3.3\times10^7\ M^{-1}s^{-1})(1.3\ mM) + 1.5\times10^4\ s^{-1}$; [8]), relative to the NMR timescale, which suggests that the observed single peak is a population-averaged peak of unbound and bound P_i. [The rate constant of P_i exchange needed to observe a population-averaged peak can be estimated from the chemical shift difference between bound (3.8 ppm, *vida infra*) and unbound (2.19 ppm, Table S3) P_i and the ^{31}P frequency (162 MHz) of the NMR spectrometer. These parameters correspond to a frequency difference of 260 Hz, above which discrete peaks for unbound and bound P_i would not be resolved. The exchange value of 6×10^4 s^{-1} estimated above is much greater than 260 s^{-1}, consistent with the observation of a single peak.] As 100% P_i binding could not be readily achieved at accessible concentrations of protein, we determined the observed chemical shift versus the fraction P_i bound and extrapolated

to estimate the chemical shift of fully bound P_i (Figure S10B). This extrapolated chemical shift is ~3.8 ppm, within error of the chemical shift of P_i bound to WT AP. The result suggests that the same P_i species are bound to both WT and R166S AP.

Text S8. ^{31}P NMR of P_i-bound to S102G and S102G/R166S AP with excess P_i

^{31}P NMR was used to probe whether multiple P_i species bind to S102G/R166S AP. Previous results with WT AP showed that the chemical shift of noncovalently bound P_i remains constant over a pH range from 5-10 [7], consistent with vibrational data that also suggest that a single P_i species binds over this pH range [7]. Similarly, the chemical shift of S102G-bound P_i does not change with pH (Figure S11A), suggesting that a single P_i species binds across this pH range. The data in the main text provide strong evidence that this species is PO_4^{3-} (see "pH-dependent P_i binding to AP without the Ser102 nucleophile" in Results and Discussion). In contrast, the ^{31}P NMR chemical shift observed for P_i in the presence of S102G/R166S AP varies systematically at different pH values (Figure 6). The single, variable chemical shift could reflect pH-dependent binding of multiple P_i-bound forms that are in rapid exchange or a rapid exchange process between bound and unbound P_i.

We distinguished between these models as follows. If the observed chemical shift reflects multiple bound P_i forms then addition of excess P_i would result in the appearance of a new peak, reflecting the added, unbound P_i. In contrast, if the observed chemical shift reflects rapid exchange binding of bound and unbound P_i then addition of excess P_i would result in a shift of the original peak toward the expected chemical shift value of unbound P_i, without the appearance of a new peak. Addition of P_i in excess of the S102G/R166S AP concentration resulted in the appearance of a new ^{31}P peak at each pH, as expected for the former model with multiple bound P_i forms. One peak had a chemical shift corresponding to the expected unbound P_i shift at that pH (see Table S3) and the other with a chemical shift corresponding to that for the sample without excess P_i (Figure S11B). The chemical shift that is observed both in the absence and presence of excess P_i is not perturbed by the presence of free P_i, strongly suggesting that this

chemical shift represents that of P_i bound to S102G/R166S AP in multiple forms whose relative populations depend on the pH of the solution.

Text S9. Equations derived from the models in Figure 4C and D to fit the pH-dependent P_i binding data for R166S (Equation S1) and S102G/R166S (Equation S2) AP in Figure 4A.

$$K_a^{P_i^{observed}} = \left(\frac{1}{1+10^{(pH-pK_a^{inactive})}}\right) \times \left(\frac{K_a^{SerO^-\bullet HPO_4^{2-}}}{\left(1+10^{(pK_a^{H_3PO_4}+pK_a^{H_2PO_4^-}-2pH)}+10^{(pK_a^{H_2PO_4^-}-pH)}+10^{(pH-pK_a^{HPO_4^{2-}})}\right)}\right) \quad \text{(Equation S1)}$$

$$K_a^{P_i^{observed}} = \left(\frac{1}{1+10^{(pH-pK_a^{inactive})}}\right) \times \left(\frac{K_a^{Gly\bullet HPO_4^{2-}}}{\left(1+10^{(pK_a^{H_3PO_4}+pK_a^{H_2PO_4^-}-2pH)}+10^{(pK_a^{H_2PO_4^-}-pH)}+10^{(pH-pK_a^{HPO_4^{2-}})}\right)} + \frac{K_a^{Gly\bullet PO_4^{3-}}}{\left(1+10^{(pK_a^{H_3PO_4}+pK_a^{H_2PO_4^-}+pK_a^{HPO_4^{2-}}-3pH)}+10^{(pK_a^{H_2PO_4^-}+pK_a^{HPO_4^{2-}}-2pH)}+10^{(pK_a^{HPO_4^{2-}}-pH)}\right)}\right) \quad \text{(Equation S2)}$$

The model in Figure 4D from which Equation S2 is derived contains a thermodynamic cycle between the solution HPO_4^{2-} and PO_4^{3-} species, the binding affinities of each species, and the S102G/R166S AP-bound equilibrium between HPO_4^{2-} and PO_4^{3-}. From the ^{31}P NMR measurements in Figure 6, the S102G/R166S AP-bound equilibrium constant ($K^{Gly\bullet P_i^{2-/3-}}$) is $10^{-6.1}$ M, and this value was used as a constraint in obtaining the fit of the pH-dependent data in Figure 4A from Equation S2 as follows. The relationship of the thermodynamic cycle in Figure 4D gives $K_a^{Gly\bullet HPO_4^{2-}} \times K^{Gly\bullet P_i^{2-/3-}} = K_a^{Gly\bullet PO_4^{3-}} \times K^{HPO_4^{2-}}$. Rearranging yields $(K_a^{Gly\bullet PO_4^{3-}})/(K_a^{Gly\bullet HPO_4^{2-}}) = (K^{Gly\bullet P_i^{2-/3-}})/(K^{HPO_4^{2-}})$ and $(K_a^{Gly\bullet PO_4^{3-}})/(K_a^{Gly\bullet HPO_4^{2-}}) = (10^{-6.1}\text{ M})/(10^{-11.7}\text{ M}) = 10^{5.6}$, and this ratio was held constant in the fit to the data in Figure 4A.